Star Formation Rate Determinations in the Milky Way and Nearby Galaxies

Daniela Calzetti[1], Kartik Sheth[2], Edward Churchwell[3], James Jackson[4]

ABSTRACT

We review measurements of star formation rates (SFRs) at multiple wavelengths, comparing indicators commonly used in Milky Way studies with those used for external galaxies, and highlighting similarities and differences. Choices of the most appropriate SFR indicators for investigations in the two environments (Milky Way versus external galaxies) are driven by basic observational differences between the two, such as the dust column density (substantially larger towards the Galactic Center than towards a typical external, unresolved or partially resolved, galaxy) and the spatial resolution. Recent progress in the calibration of mid–infrared SFR indicators enabled by the Spitzer Space Telescope is reviewed with an outlook on the expected capabilities of future missions. SFR calibrations collected from the literature, from the X–ray to the radio, are presented after re–normalization to a common Kroupa stellar initial mass function.

Subject headings: galaxies: ISM — infrared: galaxies — infrared: ISM — ISM: dust, extinction — ISM: structure

1. Introduction

Measurements of star formation rates (SFRs) provide fundamental physical parameters for characterizing galaxies and their evolution. Calibrations for SFRs have been derived at all possible wavelengths, from the X–ray to the radio, and using both continuum and

[1]Dept. of Astronomy, University of Massachusetts at Amherst

[2]CalTech/Spitzer Science Center

[3]Dept. of Astronomy, University of Wisconsin at Madison

[4]Astronomy Department, Boston University

line emission (see, e.g., Kennicutt 1998, Yun, Reddy & Condon 2001, Kewley et al. 2002, Ranalli, Comastri & Setti 2003, Bell 2003, Kewley, Geller & Jansen 2004, Calzetti et al. 2005, Schmitt et al. 2006, Moustakas, Kennicutt, & Tremonti 2006, Calzetti et al. 2007, Salim et al. 2007, Persic & Rephaeli 2007, Rosa–Gonzalez et al. 2007, Kennicutt et al. 2007).

The common challenge all calibrations share is determining how accurately the emission at a given wavelength or range of wavelengths traces the most recent star formation event (a.k.a., the most massive stars) in a system. 'Contaminants' include emission contributions to the band from older stellar populations and/or, in the case of bands that probe direct stellar light (from the ultraviolet to the near infrared), the effect of dust reddening and attenuation.

SFR indicators that measure more or less directly stellar light emission carry the added complication that different timescales may be probed at different wavelengths or in different regimes. A well known case is that of the ultraviolet (UV) emission when compared to the hydrogen recombination line emission. The UV longward of the Lyman break is photospheric emission from massive, young stars, while hydrogen recombination line emission 'counts' ionizing photons in the nebula, thus ionizing stars need to be present. A change of a factor 100 in the continuum intensity at 1500 Å occurs over a 100 Myr timescale, but the same variation in Hα flux only requires a time interval of 9 Myr for an instantaneous–burst population (Leitherer et al. 1999), since the massive stars that can produce measurable amounts of ionizing photons have considerably shorter lifetimes than massive stars that can produce UV continuum light.

In the infrared window, beyond a few μm, the continuum emission is mostly due to stellar light that has been re–processed by dust. In thermal equilibrium, the effective temperature of the dust depends on the characteristics of the dust grains and on both the energy of the stellar photons and the density of the stellar radiation field; thus the association between dust emission in a given band and massive stars is not immediate (Draine & Li 2007). Because old, evolved stellar populations can also heat the dust that radiates into the infrared, separating recent star formation from the 'contamination' of old populations is a challenge for this wavelength window that has been known since the times of the IRAS mission (e.g., Helou 1986, Lonsdale–Person & Helou 1987).

Underlying all SFR indicators is an assumption on the stellar initial mass function (IMF; e.g., Salpeter, 1955, Kroupa 2001, 2008). Since all indicators try to measure the recent star formation, they target the short–lived massive stars; thus, for most or all indicators, the low–end of the stellar IMF is a free, unconstrained parameter. Conversely, different indicators may have different sensitivity to variations of the high–end of the IMF; for instance, changing

the upper limit of the stellar IMF from 100 $M_{\odot}$to 30 $M_{\odot}$will change the intensity of the hydrogen recombination lines by a factor of 5, and the UV continuum emission at 1500 Å by a factor 2.3. In this work, we consistently adopt the Kroupa (2008) IMF, rescaling, where necessary, calibrations using other IMFs to our baseline IMF. For comparison, while the Salpeter (1955) IMF is described by a constant power law α=2.35 in the mass range 0.1–100 $M_{\odot}$, the Kroupa (2008) IMF has a shallower slope (α_1=1.3) below 0.5 $M_{\odot}$ and a high–mass slope (α_2=2.3) similar to the Salpeter one. Translating SFR indicators from the Salpeter IMF to the Kroupa IMF in the stellar mass range 0.1–100 $M_{\odot}$ implies dividing the calibration constants by ∼1.5.

A summary of calibrations as a function of wavelength is given in Table 1, where all calibration constants are re-normalized to our adopted stellar IMF.

A potential issue for SFR indicators that is not discussed in this review is the possibility that the calibrations may depend on the mass distribution of the stellar clusters formed in a galaxy. More specifically, if cluster masses are small, such as can happen in low–SFR systems, there will be a limit on the most massive stars that can be formed. This dependence, if present, will have the largest impact on the least active star–forming galaxies. The interested reader is referred to Pflamm–Altenburg et al. (2007) for further discussion.

2. Milky Way versus External Galaxies

Studies of SFR in the Milky Way and in external galaxies differ substantially in nature and in many of the tools used.

Star formation in the Milky Way is mostly located in the plane of the galaxy towards the inner disk and is, therefore, observed 'edge–on' through large dust column densities. SFR indicators at wavelengths shorter than the infrared are generally considered unreliable. Even Brγ (2.166 μm) is 'too absorbed'! Very little Galactic star formation is located in relatively transparent regions; notably, the Orion Nebula contains only 0.016% of all the massive stars in the Milky Way.

Conversely, external galaxies are observed at all possible inclinations and a non–negligible fraction of the UV light escapes from them. Although the observed UV usually needs appropriate corrections for the effects of dust extinction, approximate recipes for such corrections exist (e.g., Calzetti et al. 1994, Meurer et al. 1999, Calzetti et al. 2000) and the use of the UV or optical emission to probe SFR is fairly widespread both at low and high redshift.

The next large difference between the Milky Way and other galaxies is the spatial

Table 1: SFR Calibrations.

Waveband	SFR ($M_\odot$ yr^{-1})	Comments	Reference
X–ray	$(1.7\pm0.3)\times10^{-40}L_{2-10\ keV}$ (erg s^{-1})	SFR<50 $M_\odot$ yr^{-1}	(1), (2)
	$(8.9\pm1.8)\times10^{-40}L_{2-10\ keV}$ (erg s^{-1})	SFR$\gtrsim$50 $M_\odot$ yr^{-1} or young gals	(2)
	$(1.5\pm0.5)\times10^{-40}L_{0.2-2\ keV}$ (erg s^{-1})		(1)
UV	$(8.1\pm0.9)\times10^{-29}$ l$_\nu$ (erg s^{-1} Hz^{-1})	0.13-0.26 μm range	(3), (4)
Hα	$(5.3\pm1.1)\times10^{-42}$ L(Hα) (erg s^{-1})		(3)
MIR	1.27×10^{-38} [L(24 μm) (erg s^{-1})]$^{0.885}$	L(24 μm)= ν l(ν)	(5), (6)
	5.3×10^{-42} [L(Hα)$_{obs}$ + 0.031 L(24 μm)]	see text	(5), (7)
FIR	3.0×10^{-44} L(8-1000 μm) (erg s^{-1})	see text	(3)
Radio	4.1×10^{-21} $\nu^{0.1}$ l$_{\nu,T}$ (W Hz^{-1})	l$_{\nu,T}$=thermal emiss.	(8)
	3.5×10^{-22} $\nu^{0.8}$ l$_{\nu,NT}$ (W Hz^{-1})	l$_{\nu,NT}$=non–thermal emiss.	(8)
	4.0×10^{-22} l$_{1.4\ GHz}$ (W Hz^{-1})	l$_{1.4\ GHz}$=obs. radio luminosity	(9), (8)

Note. — References: (1) Ranalli et al. 2003; (2) Persic & Rephaeli 2007; (3) Kennicutt 1998; (4) Salim et al. 2007; (5) Calzetti et al. 2007; (6) Alonso–Herrero et al. 2006; (7) Kennicutt et al. 2007; (8) Schmitt et al. 2006; (9) Yun et al. 2001.

resolution afforded by observations. In the Milky Way, individual star forming clouds are usually easily separated from the surrounding gas/dust components and stellar populations. The high spatial scale of Milky Way observations implies that the detailed physical processes underlying massive star formation can be investigated. Conversely, in external galaxies, especially in those beyond the Local Group, limitations in the highest achievable spatial detail hinder detailed investigations of the star formation processes, and only statistical approaches are generally enabled. Milky Way studies can routinely employ SFR indicators, such as FIR and thermal radio emission, that are often difficult to use in external galaxies, where 'contaminants' (e.g., dust–heating old stellar populations in the infrared or synchrotron emission in the radio) become a concern.

In what follows, we concentrate on the SFR indicators defined in the long wavelength range in common between the Milky Way and external galaxies, i.e., the mid–to–far IR and the radio, highlighting similarities and differences of use in the two regimes.

3. Mid–Infrared Emission

Studies using ISO data provided the first window on the use of the monochromatic mid–IR (MIR, $\lambda \sim$5–40 μm) emission as a SFR indicator (e.g., Roussel et al. 2001, Boselli, Lequeux, & Gavazzi 2004, Forster–Schreiber et al. 2004, Peeters, Spoon, & Tielens 2004); investigations with the higher angular resolution and more sensitive Spitzer 8 μm and 24 μm data have expanded on the ISO results, both in the Milky Way and in external galaxies.

The use of monochromatic measures in the MIR offers a major advantage relative to the bolometric infrared emission; it is not subject to uncertain extrapolations of the IR spectral energy distribution (SED) across the full wavelength range and it is, possibly, a closer probe of the dust heated by young, hot, massive stars than the IR emission at longer wavelengths. However, whether and which of the MIR bands can effectively be used as SFR tracers is not fully settled yet.

The dust emission in the MIR wavelength range is due to both continuum and emission features. The continuum is produced by dust heated by a combination of single–photon and thermal equilibrium processes, with the latter becoming more and more prevalent at longer wavelengths (Draine & Li 2006). The MIR emission features are generally attributed to Polycyclic Aromatic Hydrocarbons (PAH, which produce a series of features in the wavelength range 3–15 μm; Leger & Puget 1984, Sellgren 1984), large molecules transiently heated by single UV and optical photons in the general radiation field of galaxies, and which can be destroyed, fragmented, or ionized in the proximity of hard UV photon fields.

3.1. The Milky Way

It has been known for sometime that massive YSOs steeply increase in luminosity from NIR to FIR wavelengths due to domination of warm, circumstellar, infalling, envelopes that convert YSO UV photons to FIR. Typically, young massive YSOs have their peak emission at about 100 μm and may exceed the radio continuum emission by a factor of 1000 or more. The detailed study of massive star formation regions in the Galaxy using both the GLIMPSE and MIPSGAL surveys (Churchwell et al. 2006) has shown that the SEDs of YSOs may have a wide range of colors from 3.6 to 24 μm due to inclinations to the line of sight of the accretion disks, the YSO evolutionary state, the presence of PAH emission features, and the YSO mass among other things. The result of this is that the use of a single set of MIR wavelength bands to identify YSOs is usually inadequate to accurately categorize all YSOs in a given star formation region. However, the addition of 24 μm emission to the four Spitzer IRAC bands has proven to be especially powerful in identifying YSOs (Robitaille et al. 2006, 2007). Practically the only other class of objects that have similar MIR SEDs to YSOs are galaxies with active star formation.

Estimating SFRs in a single massive star formation region (MSFR) using either the integrated MIR luminosity or the luminosity in a given MIR band is subject to many uncertainties, which are due to several reasons. One, the fraction of MIR luminosity that emerges from a MSFR depends on both the IMF and the upper mass cutoff of the protocluster; even under the (uncertain) assumption that the IMF is universal, the upper mass cutoff of clusters is still a function of the local conditions of the collapsing cloud. Two, the fraction of stellar luminosity that emerges, via dust heating, from MSFRs at MIR bands is very small relatively to the integrated IR emission, and a small uncertainty can result in a large error in the estimated SFR. Three, MIR bands that include PAH emission features can make a large contribution to the apparent MIR luminosity, but the strength of these features are not related to stellar effective temperatures or luminosities in any simple way as the thermal emission is; the PAH emission traces the photo–dissociation regions/bubbles (PDRs) surrounding HII regions and former HII regions/B stars, rather than the location of the massive stars (Figure 1; Churchwell et al. 2006, Watson et al. 2008). Four, as with all cluster photometry, one has to correct for background emission and judge where the boundaries of a MSFR occur to obtain its MIR luminosity, even if its distance is known; both of these are fraught with difficulty and introduce relatively large errors, which as noted above adds to the uncertainty in MIR luminosity and in any SFR relation that depends on this quantity.

However, there is also evidence for a strong spatial correlation between strong MIR emission and presence of MSFRs. Examination of the GLIMPSE and MIPSGAL surveys

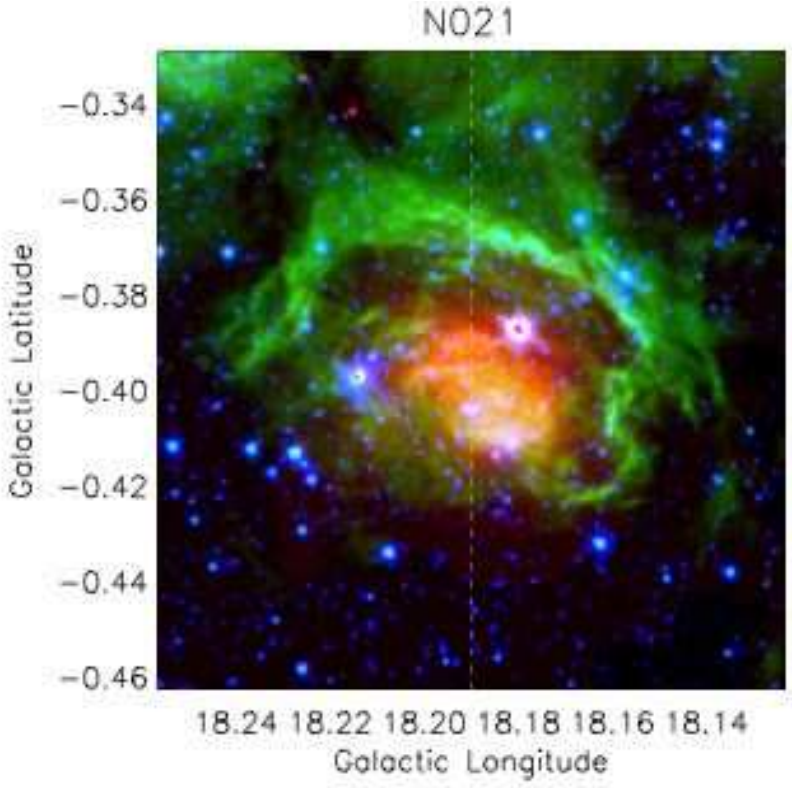

Fig. 1.— Color–composite image of the Galactic HII region/bubble N021 (reproduced with permission from Watson et al. 2008), showing the relative distribution of the 8 μm emission (green, tracing the PDR surrounding the HII region), the 24 μm emission (red, tracing the dust heated by the massive star(s)), and the 4.5 μm emission (blue, tracing the stars). The image shows strikingly the spatial separation between the peak of the hot dust emission and the highest intensity 8 μm emission region.

show very clearly that dust in the neighborhood of a MSFR lights up like a neon sign due to both PAH emission (at 5.8 and 8.0 μm) and thermal emission at 24 μm. Robitaille et al. (2006, 2007) have demonstrated that it is possible to identify and estimate the evolutionary state of YSOs by combining multi–wavelength (NIR–MIR) data with YSO monte carlo radiative transfer models (Whitney et al. 2003a, b, 2004; Indebetouw et al. 2007) and realistic 3D morphologies. The Robitaille et al. models have been tested against known YSOs in Taurus and found to reliably reproduce the observed SEDs and to give reliable estimates of evolutionary class, visual extinction, mass, and other physical properties of the known YSOs. As our knowledge of YSO properties improve, they can be incorporated into the input model parameters to tighten the determination of YSO properties with evolutionary state.

3.2. External Galaxies

Investigations of MIR emission from external galaxies mirror, in a spatially–integrated fashion, many of the complexities observed in the massive star formation regions of the Milky Way.

The MIR bands containing the PAH features have been shown to correlate with the number of ionizing photons emerging from galaxy disks and the nuclear regions of galaxies (Roussel et al. 2001, Forster-Schreiber et al. 2004). Indeed, for restricted choices of galactic parameters (e.g., disks with solar metallicity), the PAH emission as traced by the Spitzer 8 μm band correlates almost linearly with the SFR (Calzetti et al. 2007).

However, analyses including a wider range of galaxy properties show that the PAH emission also trace closely dust heated by evolved stellar populations not linked to current star formation (Haas et al. 2002, Boselli et al. 2004, Calzetti et al. 2007, Bendo et al. 2008), its correlation with tracers of ionizing photons is shallower than unity (Wu et al. 2005, Calzetti et al. 2005), and, similarly to what is observed in our Milky Way, the PAH emission traces more closely the PDRs surrounding the HII regions, rather than the HII regions themselves (Helou et al. 2004, Bendo et al. 2006). Worse yet, the strength of the PAH emission is a strong function of metallicity (Boselli et al. 2004, Engelbracht et al. 2005, Draine & Li 2007): regions with 1/10 $Z_{\odot}$ are about 30 times fainter at 8 μm than regions with solar metallicity (Calzetti et al. 2007), which is possibly an effect of destruction by harder radiation fields in lower metallicity galaxies (Madden et al. 2006).

Conversely, the continuum emission at 24 μm (the shortest wavelength band of Spitzer/MIPS) has been shown to be a closer tracer of ionizing photons than the PAH emission (Calzetti et al. 2005, Wu et al. 2005, Perez–Gonzalez et al. 2006, Alonso–Herrero et al. 2006, Calzetti et al. 2007), possibly because it includes a larger fraction of thermal emitting dust than shorter MIR wavelengths. Caveats include: sensitivity to the presence of AGNs (which heat the dust at high temperatures, thus emitting strongly at 24 μm), and a modest sensitivity, at the level of a factor 2–4, to metallicity, the latter fully accounted for by the increased transparency of the medium at lower metal abundances. With these caveats in mind, a calibration for SFR using the 24 μm monochromatic emission can be defined over 3.5 orders of magnitude (Figure 2, left; Calzetti et al. 2007):

$$SFR_{MIR}(M_{\odot}\ yr^{-1}) = 1.27 \times 10^{-38}[L(24\ \mu m)\ (erg\ s^{-1})]^{0.885}, \quad (1)$$

where the luminosity L(24 μm)=νl(ν). The non–linear correlation between the SFR and the 24 μm luminosity is a direct consequence of the proportionally higher dust temperature in more actively star forming objects, which causes a larger fraction of the IR dust emission to emerge at MIR wavelengths (Draine & Li 2007).

One of the limitations in using a dust–emission–based SFR indicator is that it becomes unreliable in conditions of low–dust content (Cannon et al. 2006, Walter et al. 2007). This limitation can be offset by combining the MIR emission at 24 μm with a tracer of the ionizing photons that has *not* been absorbed by dust: this tracer is the *observed* (i.e., not extinction–corrected) Hα emission. The observed 24 μm and Hα luminosities of an extragalactic object can be combined to provide a SFR diagnostic via (Kennicutt et al. 2007, Calzetti et al. 2007):

$$SFR(M_{\odot}\ yr^{-1}) = 5.3 \times 10^{-42}[L(H\alpha)_{obs} + (0.031 \pm 0.006)L(24\ \mu m)]. \quad (2)$$

This diagnostic is unaffected by dust (metals) content (Figure 2, right), but shows a deviation from a purely linear correlation at high luminosities, which reflects the non–linearity of the 24 μm luminosity with SFR (equation 1) when the latter becomes the dominant contribution to equation 2. The above relation, although in principle useful in studies of low–redshift galaxies, thanks to the many extensive surveys performed by the Spitzer Space Telescope, may be difficult to apply at high redshift, where the restframe Hα and 24 μm emission are often not simultaneously available.

4. Far–Infrared Emission

SFR diagnostics in the far–infrared region of the spectrum (λ ∼40–500 μm) mainly involve, at least to date, the use of the bolometric IR emission, integrated in the range ∼8–1000 μm, L(8-1000 μm), or of ISM cooling lines such as the [CII](λ158 μm) and the [NII](205 μm).

The bolometric IR emission simply measures the entire output from the dust heated by the stellar populations. Because of the increasing dust opacity at decreasing wavelengths, UV photons will be more absorbed by dust than optical or IR photons; thus, in the case of a star–forming region or an actively star–forming galaxy, dust emission is effectively a measure of the UV output of the system. The two underlying assumptions in the previous statement are that: (1) the young stellar populations dominate the bolometric stellar output from the system; (2) there is enough dust to absorb most of the UV photons. If both assumptions are true, a useful calibration is given in Kennicutt (1998), which we reproduce for our baseline IMF:

$$SFR_{FIR}(M_{\odot}\ yr^{-1}) = 3.0 \times 10^{-44} L(8 - 1000\ \mu m)\ (erg\ s^{-1}). \quad (3)$$

The above relation is routinely applied to Milky Way obscured MSFRs, because the high spatial resolution afforded by proximity enables the separation of the star–forming regions from surrounding stellar populations, which produces 'clean' SFR measurements. The MSFRs are often identified using molecular or dense gas tracers and FIR data from IRAS or

COBE are then used to measure SFRs (e.g., Luna et al. 2006).

In external galaxies, star–forming populations are generally not easy to separate from older stellar populations because of the lower spatial resolution. This generates a 'contamination' for the calibration in equation 3, in the sense that the IR emission from the galaxy will be artificially enhanced due to dust heating by evolved populations; in this case, the IR probes timescales much longer than those pertaining to recent star–formation, and the 'contamination' likely increases with wavelength. The opposite trend, i.e. an artificial decrease in the SFR estimate, happens in the rather frequent case that galaxies are not completely obscure in the UV; in this case, part of the UV emission emerges from the galaxy, leading to an underestimate of SFR_{FIR} (see discussion in Kennicutt 1998). A recent attempt to statistically correct for both effects in samples of nearby galaxies, i.e. contamination from old stellar populations and leakage of unabsorbed UV photons, is due to Bell (2003), providing the following calibration for our IMF:

$$\begin{aligned} SFR_{FIR}(M_\odot\ yr^{-1}) &= 2.7\times10^{-44}\Big[1+\Big(\frac{3.9\times10^{42}}{L_{FIR}}\Big)^{0.5}\Big]L_{FIR}, \quad L_{FIR} > 3.9\times10^{44} \\ &= 2.0\times10^{-44}\Big[1+\Big(\frac{3.9\times10^{42}}{L_{FIR}}\Big)^{0.5}\Big]L_{FIR}, \quad L_{FIR} \leq 3.9\times10^{44} \quad (4) \end{aligned}$$

where L_{FIR}=L(8–1000 μm) is in units of erg s^{-1}. The scatter on the above relations (equation 4) is at least a factor of 2, and application to individual galaxies can lead to much larger errors (Bell 2003).

Distant galaxies present additional complications: SFR_{FIR} requires an estimate of the *bolometric* output in the IR, which involves measurements at multiple wavelengths and is often difficult to obtain for high–redshift objects; extrapolations of L(8–1000 μm) from one or two measurements are generally highly uncertain, especially if those measurements are far from the peak emission.

Infrared cooling lines are potentially powerful tracers of SFR because they are not as sensitive to dust extinction as, e.g., optical emission lines. The strongest emission line in the FIR regime is [CII](λ158 μm), and this line has been extensively investigated both in the Milky Way and in external galaxies because of its high potential to provide an unbiased SFR indicator. [CII] is likely the strongest cooling line in the ISM of galaxies, having comparable or stronger intensity than the Hα emission (Smith 2008).

For the Milky Way, COBE has provided excellent maps of both [CII](λ158 μm) and [NII](λ205 μm) (e.g. Fixsen, Bennett & Mather 1999). The [CII]/FIR emission varies widely across our Galaxy, from a few percent down to a few hundredths of percent, a finding that supports the suggestion that [CII] may be the dominant coolant of several phases of the

ISM, being associated with PDRs, the warm ionized medium and the cold neutral medium (Madden et al. 1993, Fixsen et al. 1999, Abel 2006). Conversely, [NII] appears to be mainly associated with the warm ionized medium, implying that it can be utilized to 'count' ionizing photons, and is an excellent, extinction–free proxy for SFR (Bennett et al. 1994).

Because of its intensity, [CII] is a strong candidate for tracing SFRs in external galaxies; [NII] is many times fainter than [CII], thus much more difficult to detect and use. ISO brought a major 'push' in the investigation of [CII] as a SFR tracer (e.g. Fischer et al. 1999, Malhotra et al. 2001, Contursi et al. 2002, and references therein). Although the [CII]/FIR ratio was found to be roughly constant in a number of galaxies, suggesting that [CII] may be mainly probing PDRs in the spatially–integrated external galaxies (Malhotra et al. 2001, see also Rodrigues–Fernandez et al. 2006), significant deviations from this trend were observed both in detailed maps of galaxies (e.g., Contursi et al. 2002) and in some classes of galaxies (e.g., ULIRGs, Fischer et al. 1999). There may be multiple reasons for the deviations, including optically–thick or collisionally de–excited [CII], and/or old–stars contributions to the FIR emission (Malhotra et al. 2001). For this issue, the next quantum leap will be provided by the Herschel Space Telescope, which is far superior to ISO both in angular resolution and sensitivity; a number of Guaranteed Time and Open Time projects have the investigation of [CII] as a SFR indicator among their goals.

5. Radio Emission

The radio ($\lambda \sim$cm) emission from star forming regions and galaxies is a combination of thermal (free–free, tracing the total number of ionizing photons) and non–thermal (synchrotron from cosmic ray electrons, tracing supernova remnants) emission.

In the spatially resolved star–forming regions of the Milky Way, HII regions can be separated from supernova remnants (SNRs), thus enabling a discrimination of the two contributions to the radio emission. In this regime, the thermal radio emission can be effectively used as a SFR tracer. A recent calibration of the thermal emission, from Schmitt et al. (2006), is re-produced here using our baseline stellar IMF:

$$SFR_{RT}(\ M_{\odot}\ yr^{-1}) = 4.1 \times 10^{-21} \nu^{0.1} l_{\nu,T}, \tag{5}$$

where SFR_{RT} is the SFR derived from the thermal radio emission, $\mathrm{l}_{\nu,T}$ is the thermal radio luminosity in units of W Hz^{-1}.

In external galaxies, separation of thermal and non–thermal emission is difficult to achieve, and can usually be done only with multi–wavelength radio observations (e.g., Reines, Johnson & Goss 2008) on spatially–averaged regions. Yet, the tight correlation between

the radio emission at ν $\sim$1 GHz (mostly synchrotron) and the far–infrared emission of galaxies (de Jong et al. 1985, Condon 1992, Murphy et al. 2006) justifies the definition of a SFR indicator from the mostly–non–thermal radio emission of mostly unresolved galaxies, although the underlying physical mechanism for the correlation is not completely clear yet (e.g., Murphy et al. 2006).

Using our adopted stellar IMF, we extrapolate from the calibration of Schmitt et al. (2006), to obtain:

$$SFR_{RNT}(\ M_{\odot}\ yr^{-1}) = 3.5 \times 10^{-22} \nu^{0.8} l_{\nu,NT}, \tag{6}$$

where $l_{\nu,NT}$ is the non–thermal radio luminosity in units of W Hz^{-1}. The above relation, which traces SNRs, will in general not be applicable to very young or 'nascent' ($\lesssim$30–50 Myr) starbursts or star–forming systems. In the case of integrated radio flux from galaxies, where the separation of thermal from non–thermal radio emission is difficult or not possible, SFRs at specific wavelengths can be calibrated (Yun et al. 2001, Schmitt et al. 2006); for instance at 1.4 GHz (λ=20 cm):

$$SFR_{1.4\ GHz}(\ M_{\odot}\ yr^{-1}) = 4.0 \times 10^{-22} l_{1.4\ GHz}, \tag{7}$$

where $l_{1.4\ GHz}$ is the *total* measured radio luminosity, in units of W Hz^{-1}.

A new step in the quest for unbiased SFR indicators will be the exploration of extinction–free hydrogen recombination lines at sub–millimiter/millimiter wavelengths using new facilities, like ALMA and the Large Millimiter Telescope (Yun 2007).

6. Summary and Conclusions

Progress in the calibration of SFR indicators at a variety of wavelengths, from the X–ray to the radio, has closely followed over the past few years the availability of large, homogeneous data and samples from a number of both old and recent space missions, such as Spitzer, Chandra, XMM–Newton, HST, GALEX. In this contribution, we have summarized the calibration of SFR indicators from the X–ray to the radio from recent literature, re–normalizing all calibrations to the recent Kroupa stellar initial mass function. The expectation is that further progress will be pushed by upcoming missions, such as Herschel, ALMA, LMT, JWST, and others.

Star formation in the Milky Way, being concentrated in the galactic disk, is located behind substantially large dust column densities, due to our specific observational location. The implication is that the Milky Way's star formation can be studied only at wavelengths longer than a few μm (or in the X–rays). This is different from external galaxies, which,

being observed from the 'outside', do 'shine' also at short wavelengths, such as the UV and optical, and star formation can be reliably investigated at these wavelengths. However, the Milky Way has the undeniable advantage that observations have a much higher spatial resolution than those of external galaxies, thus star formation processes can be investigated in greater detail, and with better control of 'contaminants', such as old stellar populations contributing to the emission in one or more wavebands of interest. With an eye to these differences, we have reviewed SFR indicators at mid–IR, far–IR, and radio wavelengths, highlighting overlaps and differences of use. The sensitivity and angular resolution of the Spitzer Space Telescope at mid–IR wavelengths has been key in establishing how effective this wavelength range is in tracing the recent star formation.

This work is based on observations made with the *Spitzer Space Telescope*, which is operated by the Jet Propulsion Laboratory (JPL), California Institute of Technology under NASA contract 1407.

REFERENCES

Abel, N.P. 2006, MNRAS, 368, 1949

Alonso–Herrero, A., Rieke, G.H., Rieke, M.J., Colina, L., Perez-Gonzalez, P.G., & Ryder, S.D. 2006, ApJ, 650, 835

Bell, E.F. 2003, ApJ, 586, 794

Bendo, G.J., Dale, D.A., Draine, B.T., Engelbracht, C.W., Kennicutt, R.C., Calzetti, D., Gordon, K.D., Helou, G., Hollenbach, D., Li, AIgen, Murphy, E.J., et al. 2006, ApJ, 652, 283

Bendo, G.J., Draine, B.T., Engelbracht, C.W., Helou, G., Thornley, M.D., Bot, C., Buckalew, B.A., Calzetti, D., Dale, D.A., Hollnbach, D.J., Li, A., & Moustakas, J. 2008, MNRAS, accepted

Bennett, C.L., Fixsen, D.J., Hinshaw, G., Mather, J.C., Moseley, S.H., Wright, E.L., et al. 1994, ApJ, 434, 587

Boselli, A., Lequeux, J., & Gavazzi, G. 2004, A&A, 428, 409

Calzetti, D., Armus, L., Bohlin, R.C., Kinney, A.L., Koornneef, J., & Storchi-Bergmann, T. 2000, ApJ, 533, 682

Calzetti, D., Kennicutt, R.C., Bianchi, L., Thilker, D.A., Dale, D.A., Engelbracht, C.W., Leitherer, C., Meyer, M.J., et al. 2005, ApJ, 633, 871

Calzetti, D., Kennicutt, R.C., Engelbracht, C.W., Leitherer, C., Draine, B.T., Kewley, L., Moustakas, J., Sosey, M., et al. 2007, ApJ, 666, 870

Calzetti, D., Kinney, A.L., & Storchi–Bergmann, T. 1994, ApJ, 429, 582

Cannon, J.M., Walter, F., Armus, L., Bendo, G.J., Calzetti, D., Draine, B.T., Engelbracht, C.W., Helou, G., Kennicutt, R.C., Leitherer, C., et al. 2006, ApJ, 652, 1170

Churchwell, E., Povich, M.S., Allen, D., Taylor, M.G., Meade, M.R., Babler, B.L., Indebetouw, R., Watson, C., Whitney, B.A., Wolfire, M.G., et al. 2006, ApJ, 649, 759

Contursi, A., Kaufman, M.J., Helou, G., Hollenbach, D.J., Brauher, J., Stacey, G.J., Dale, D.A., Malhotra, S., et al. 2002, AJ, 124, 751

Draine, B.T., & Li A. 2007, ApJ, 657, 810

Engelbracht, C.W., Gordon, K.D., Rieke, G.H., Werner, M.W., Dale, D.A., & Latter, W.B. 2005, ApJ, 628, 29

Fischer, J., Luhman, M.L., Satyapal, S., Greenhouse, M.A., Stacey, G.J., Bradford, C.M., Lord, S.D., et al. 1999, Ap&SS, 266, 91

Fixsen, D.J., Bennett, C.L., & Mather, J.C. 1999, ApJ, 526, 207

Förster Schreiber, N.M., Roussel, H., Sauvage, M., & Charmandaris, V., 2004, A&A, 419, 501

Haas, M., Klaas, U., & Bianchi, S. 2002, A&A, 385, L23

Helou, G. 1986, ApJ, 311, L33

Helou, G., Roussel, H., Appleton, P., Frayer, D., Stolovy, S., Storrie–Lombardi, L., Hurst, R., Lowrance, P., et al. 2004, ApJS, 154, 253

Indebetouw, R. ,et al. 2007, ApJ, 666, 321

Kennicutt, R.C. 1998, ARA&A, 36, 189

Kennicutt, R.C., Calzetti, D., Walter, F., Helou, G., Hollenbach, D.J., Armus, L., Bendo, G., Dale, D.A., Draine, B.T., Engelbracht, C.W., et al. 2007, ApJ, 671, 333

Kroupa, P. 2001, MNRAS322, 231

Kroupa, P. 2008, in Pathways through an Eclectic Universe, J.H. Knapen, T.J. Mahoney, & A. Vazdekis eds., ASP Conference Series, 390, 3

Kewley, L.J., Geller, M.J., Jansen, R.A., & Dopita, M.A. 2002, AJ, 124, 3135

Kewley, L.J., Geller, M.J., & Jansen, R.A. 2004, AJ, 127, 2002

Leger, A., & Puget, J.L. 1984, A&A, 137, L5

Leitherer, C., Schaerer, D., Goldader, J.D., González Delgado, R.M., Robert, C., Kune, D.F., de Mello, D.F., Devost, D., & Heckman, T.M. 1999, ApJS, 123, 3

Luna, A., Bronfman, L., Carrasco, L., & May, J. 2006, ApJ, 641, 938

Lonsdale Persson, C.J., & Helou, G.X. 1987, ApJ, 314, 513

Madden, S.C., Galliano, F., Jones, A.P., & Sauvage, M. 2006, A&A, 446, 877

Madden, S.C., Geis, N., Genzel, R., Herrmann, F, Jackson, J., Poglitsch, A., Stacey, G.J., & Townes, C.H. 1993, ApJ, 407, 579

Malhotra, S., Kaufman, M.J., Hollenbach, D., Helou, G., Rubin, R.H., Brauher, J., Dale, D., Lu, N.Y., Lord, S., et al. 2001, ApJ, 561, 766

Meurer, G.R., Heckman, T.M., & Calzetti, D. 1999, ApJ, 521, 64

Moustakas, J., Kennicutt, R.C., & Tremonti, C.A. 2006, ApJ, 642, 775

Peeters, E., Spoon, H.W.W., & Tielens, A.G.G.M. 2004, ApJ, 613, 986

Perez–Gonzalez, P.G., Kennicutt, R.C., Gordon, K.D., Misselt, K.A., Gil de Paz, A., Engelbracht, C.W., Rieke, G.H., Bendo, G.J., Bianchi, L., Boissier, S., Calzetti, D., Dale, D.A., et al. 2006, ApJ, 648, 987

Persic, M., & Rephaeli, Y. 2001, A&A, 463, 481

Pflamm-Altenburg, J., Weidner, C., & Kroupa, P. 2007, ApJ, 671, 1550

Ranalli, P., Comastri, A., & Setti, G. 2003, A&A, 399, 39

Reines, A.E., Johnson, K.E., & Goss, W.M. 2008, AJ, in press (astroph/0804.0005)

Robitaille, T. P., Whitney, B. A., Indebetouw, R., & Wood, K, 2007, ApJ, 169, 32

Robitaille, T. P., Whitney, B. A., Indebetouw, R., Wood, K., & Densmore, P. 2006, ApJS, 167, 256

Rodriguez–Fernandez, N.J., Braine, J., Brouillet, N., & Combes, F. 2006, A&A, 453, 77

Rosa–Gonzalez, D., Burgarella, D., Nandra, K., Kunth, D., Terlevich, E., & Terlevich, R. 2007, MNRAS, 379, 357

Roussel, H., Sauvage, M., Vigroux, L., & Bosma, A. 2001, A&A, 372, 427

Salim, S., Rich, M.R., Charlot, S., Brinchmann, J., Johnson, B.D., Schminovich, D., Seibert, M., Mallery, R., Heckman, T.M., Forster, K., et al. 2007, ApJS, 173, 267

Schmitt, H.R., Calzetti, D., Armus, L., Giavalisco, M., Heckman, T.M., Kennicutt, R.C., Leitherer, C., & Meurer, G.R. 2006, ApJ, 643, 173

Sellgren, K. 1984, ApJ, 277, 623

Smith, J.D.T. 2008, in 'Far Infrared Astronomy from SPace: A Community Workshop about the Future' (Spitzer Science Center, Pasadena, May 28-31, 2008)

Walter, F., Cannon, J.M., Roussel, H., Bendo, G.J., Calzetti, D., Dale, D.A., Draine, B.T., Helou, G., Kennicutt, R.C., Moustakas, J., et al. 2007, ApJ, 661, 102

Watson, C., Povich, M.S., Churchwell, E.B., Babler, B.L., Chunev, G., Hoare, M., Indebetouw, R., Meade, M.R., Robitaille, T.P., & Whitney, B.A. 2008, ApJ, in press (astroph/0806.0609)

Whitney, B. A. Wood, K., Bjorkman, J. E., & Wolff, M. J. 2003a, ApJ, 591, 1049

Whitney, B. A. Wood, K., Bjorkman, J. E., & Cohen, M. 2003b, ApJ, 598, 1079

Whitney, B. A., Indebetouw, R., Bjorkman, J. E., & Wood, K. 2004, ApJ, 617, 1177

Wu, H., Cao, C., Hao, C.-N., Liu, F.-S., Wang, J.-L., Xia, X.-Y., Deng, Z.-G., & Young, C. K.-S. 2005, ApJ, 632, L79

Yun, M. S., Reddy, N.A., Condon, J.J. 2001, ApJ, 554, 803

Yun, M.S., 2007, Ap&SS, 313, 253

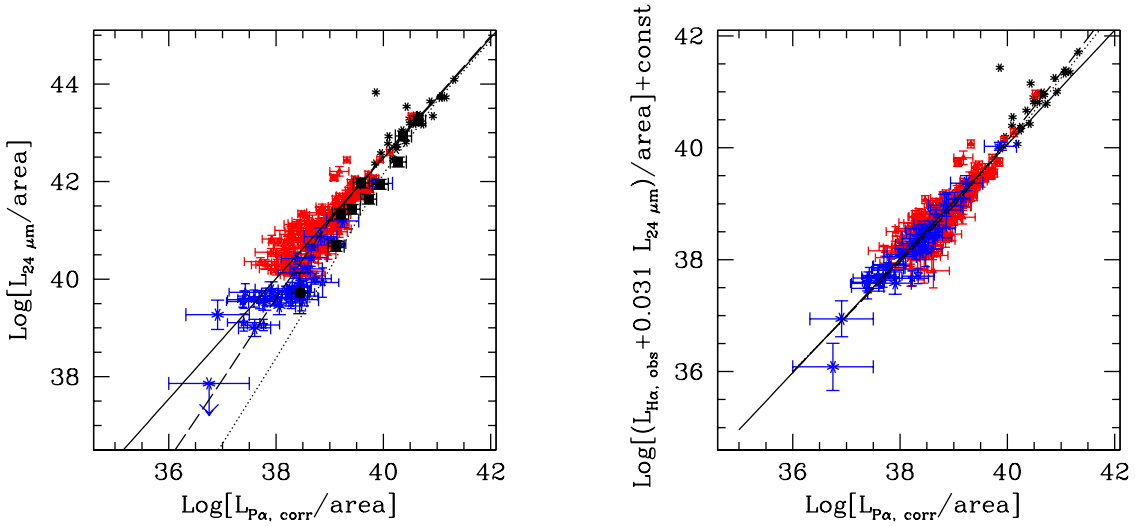

Fig. 2.— **(Left)** The luminosity per unit area, in units of erg s^{-1} kpc^{-2}, at 24 μm (from Spitzer/MIPS) and Pα (from HST/NICMOS) for a sample 220 star–forming regions in 33 nearby galaxies (red and blue symbols), 10 nearby starburst galaxies (black squares) and 24 Luminous Infrared Galaxies (LIRGS, black asterisks), from Calzetti et al. 2007. The extinction–corrected Pα line emission (λ=1.876 mm) is used here as an unbiased tracer of massive stars SFR. Of the 220 regions, the ∼180 regions in high–metallicity galaxies, 12+log(O/H)>8.3, are marked in red, and the ∼40 regions in low–metallicity galaxies are in blue. The continuous line is the best fit through the high–metallicity star–forming regions. Models for a young stellar population with increasing amount of star formation and dust are shown as a dash line ($Z=Z_{\odot}$) and a dot line ($Z=1/10\ Z_{\odot}$), using the stellar population models of Leitherer et al. (1999) and the dust models of Draine & Li (2007). The spread in the datapoint around the best fit line is well accounted for by a spread in the stellar population's age in the range 2–8 Myr. **(Right)** The same as the left panel, for the combination of Hα (observed) and 24 μm emission; the linearity of the data across most of the dynamical range shows that this SFR indicator is robust against variations in the metal/dust content of galaxies.